Assessing Responses and Impacts of Solar climate intervention on the Earth system with stratospheric aerosol injection (ARISE-SAI): protocol and initial results from the first simulations

Jadwiga H. Richter[1], Daniele Visioni[2], Douglas G. MacMartin[2], David A. Bailey[1], Nan Rosenbloom[1], Brian Dobbins[1], Walker R. Lee[2], Mari Tye[1], Jean-Francois Lamarque[1]

[1] Climate and Global Dynamics Laboratory, National Center for Atmospheric Research, Boulder CO, USA
[2] Sibley School for Mechanical and Aerospace Engineering, Cornell University, Ithaca NY, USA

Correspondence to: Jadwiga H. Richter (jrichter@ucar.edu)

Abstract. Solar climate intervention using stratospheric aerosol injection is a proposed method of reducing global mean temperatures to reduce the worst consequences of climate change. A detailed assessment of responses and impacts of such an intervention is needed with multiple global models to support societal decisions regarding the use of these approaches to help address climate change. We present here a new modeling protocol aimed at simulating a plausible deployment of stratospheric aerosol injection and reproducibility of simulations using other Earth system models, Assessing Responses and Impacts of Solar climate intervention on the Earth system with stratospheric aerosol injection (ARISE-SAI). The protocol and simulations are aimed at enabling community assessment of responses of the Earth system to solar climate intervention. ARISE-SAI simulations are designed to be more policy relevant than existing large ensembles or multi-model simulation sets. We describe in detail the first set of ARISE-SAI simulations, ARISE-SAI-1.5, which utilize a moderate emissions scenario, introduce stratospheric aerosol injection at ~ 21.5 km in year 2035, and keep global mean surface air temperature near 1.5ºC above the pre-industrial value utilizing a feedback or control algorithm. We present here the detailed set-up, aerosol injection strategy, and preliminary climate analysis from a 10-member ensemble of these simulations carried out with the Community Earth System Model, version 2 with the Whole Atmosphere Community Climate Model version 6 as its atmospheric component.

1 Introduction

Solar climate intervention (SCI), or solar radiation modification, is a proposed strategy that could potentially reduce the adverse effects on weather and climate associated with climate change by increasing the reflection of sunlight by particles and clouds in the atmosphere. The recent National Academies of Sciences, Engineering and Medicine (NASEM) report on solar geoengineering research and governance (NASEM, 2021) calls for increased research to understand the benefits, risks and impacts of various SCI approaches. Stratospheric aerosol injection (SAI), which

aims to mimic the effects of volcanic eruptions on climate, has been shown to be a promising method of global climate intervention in terms of restoring climate to present day conditions in global climate or Earth system models (e.g.: Tilmes et al., 2018; MacMartin et al. 2019; Simpson et al., 2019). However, there still exist large uncertainties in climate response and impacts (NASEM, 2021, Kravitz and MacMartin, 2020), and ensuing human and ecological impacts (Carlson and Trisos, 2018). Due to the large internal variability of Earth's climate, the evaluation of SCI risks and impacts requires large ensembles of simulations (Deser et al., 2012; Kay et al., 2015; Maher et al., 2021) and Earth system models (ESMs) capable of simulating the key processes and interactions between multiple Earth system components, including prognostic aerosols, interactive chemistry, and coupling between the atmosphere, land, ocean, and sea ice. For studies of climate intervention using SAI, an accurate representation of the entire stratosphere, including dynamics and chemistry, is needed to capture the transport of aerosols and their interactions with stratospheric constituents such as water vapor and ozone (e.g.: Pitari et al., 2014).

The Geoengineering Model Intercomparison Project (GeoMIP) for many years has facilitated inter-model comparisons of possible climate responses to SCI to examine where model responses to geoengineering were robust and identify areas of large uncertainty. However, in order to ensure participation from multiple ESMs, the design of GeoMIP simulations has often been simplified by utilizing solar constant reduction (Kravitz et al., 2013; Kravitz et al., 2021) or prescription of an aerosol distribution (Tilmes et al., 2015) or a spatially uniform injection rate of SO_2 (i.e. continuous injection from 10ºN to 10ºS in the most recent G6sulfur experiments (Visioni et al., 2021b). Visioni et al. (2021a) showed that solar dimming does not produce the same surface climate effects as simulating aerosols in the stratosphere. Kravitz et al. (2019) showed that strategically injecting SO_2 at multiple locations to maintain more than one climate target may reduce some of the projected side-effects by more evenly cooling at all latitudes; hence, model experiments with plausible implementation of SCI are needed in order to assess risks and benefits of these strategies.

The Geoengineering Large Ensemble (GLENS, Tilmes et al. 2018), which used version 1 of the Community Earth System Model with the Whole Atmosphere Community Climate Model as its atmospheric component (CESM1(WACCM), Mills et al. 2017), was the first large-ensemble (20-member) set of climate intervention simulations carried out with a single ESM that interactively represented many of the key processes relevant to SAI and has provided a community dataset for the examination of potential impact of SAI on mean climate and variability. GLENS utilized sulfur dioxide (SO_2) injections that were strategically placed every year to keep the global mean temperature, equator-to-pole, and pole-to-pole temperature gradients near 2020 levels in an effort to minimize the surface temperature impacts of this intervention. However, GLENS has several experimental design issues that are not aligned with realistic projections for Earth system outcomes that would provide more accurate representation of possible real-world effects and impacts. Firstly, GLENS adopted a high emission scenario of RCP8.5 until 2100, requiring a very large amount of stratospheric aerosols by the end of the century to offset the continuously increasing emissions. Estimates for future emissions based on current commitments are lower than RCP8.5 (Hausfather and Peters, 2020), and thus impact analyses, especially based on the last two decades of the GLENS, are likely to overestimate the risks and adverse impacts of SAI. Additionally, in the GLENS simulations, intervention commenced

in 2020, adding another unrealistic element from a real-world standpoint. Furthermore, SO_2 injections were at 23-25 km altitude, which is technologically more difficult to achieve than a lower altitude injection (Bingaman et al. 2020).

Tilmes et al. (2020) has carried out simulations with SO_2 injections with CESM2(WACCM6) and GLENS-like set-up for the Shared Socioeconomic Pathway SSP5-8.5 and SSP5-3.4-OS scenarios (O'Neill et al., 2016). Here we propose a new SAI modeling protocol for a suite of simulations designed to simulate a more plausible implementation scenario of SCI using SAI that can be replicated by other modeling centers. We denote the entire set of current and future simulations conducted under this protocol as "Assessing Responses and Impacts of Solar climate intervention on the Earth system," or "ARISE," with simulations of SAI denoted "ARISE-SAI". We anticipate that in the future similar simulations utilizing other climate intervention methods such as Marine Cloud Brightening (MCB) or Carbon Dioxide Removal (CDR), will result in ARISE-MCB or ARISE-CDR simulations respectively. In addition, we present preliminary results from the first set of these simulations carried out with the Community Earth System Model, version 2 with the Whole Atmosphere Community Climate Model version 6 as its atmospheric component (CESM2(WACCM6)). The paper is structured as follows: section 2 provides an overview of ARISE-SAI protocol including ARISE-SAI-1.5, section 3 describes the model used to describe the realization of ARISE-SAI-1.5 with CESM2(WACCM6), section 4 shows surface temperature and precipitation in these simulations, and section 5 offers a summary and conclusions.

2 ARISE-SAI

2.1 Reference Simulations

Evaluation of impacts of SCI requires a set of non-SCI reference simulations to enable comparison of impacts with and without SAI. As motivated by MacMartin et al (2022), we use here the moderate Shared Socioeconomic Pathway scenario of SSP2-4.5 for our simulations, which more closely captures current policy scenarios compared to higher emission scenarios such as SSP5-8.5 (Burgess et al., 2020). SSP2-4.5, which marks a continuation of the Representative Concentration Pathway 4.5 (RCP4.5) scenario, is a "middle-of-the-road," intermediate mitigation scenario where "the world follows a path in which social, economic, and technological trends do not shift markedly from historical patterns" (O'Neill et al., 2017), representing the medium range of future forcing pathways (O'Neill et al., 2016).

2.2 Protocol Overview

The ARISE-SAI simulations are designed to simulate a plausible implementation scenario of SCI using SAI for evaluation of potential climate intervention risks and impacts. MacMartin et al. (2022) described in detail the need for various scenarios to evaluate impacts of SCI and five dimensions of SCI deployment options which include the background climate-change scenario, desired target of cooling, start date of deployment, how cooling is achieved, and other factors that could affect decisions. The proposed default ARISE-SAI protocols follow closely the recommended scenario choices described in MacMartin et al. (2022) and describe details of implementation in Earth system models, although different choices can be made in the future to expand the simulation set. In particular, the proposed ARISE-

SAI simulations utilize a moderate emission scenario, SSP2-4.5 (O'Neill et al., 2016) and cool the Earth to a global mean temperature target (TT) above preindustrial levels denoted in the specific name of the simulations (e.g.: ARISE-SAI-TT). For example, ARISE-SAI-1.5 and ARISE-SAI-1.0 simulations aim to maintain global surface temperatures at ~1.5°C and ~1.0°C above preindustrial levels respectively.

The protocol in the first ARISE-SAI simulations (without a delayed start) simulates deployment beginning in 2035 after the global surface temperature reaches ~1.5°C above preindustrial levels, the target proposed in the 2015 Paris agreement and described by the IPCC as an important threshold for climate safety (IPCC 2018). Simulations are carried out for 35 years (2035 - 2069), which is sufficient to consider both a transition period of ~10 years and a quasi-equilibrium of at least 20 years after the controller converges. Minimum recommended ensemble size is 3, although more members will allow for more thorough evaluation of impacts on variability.

2.3 ARISE-SAI-1.5

The first ARISE-SAI simulations, ARISE-SAI-1.5 presented here, aim to keep the global mean temperature at ~1.5°C above pre-industrial levels. There is uncertainty among Earth system models with regard to when Earth's global mean surface temperature (T0) will reach 1.5°C above pre-industrial levels. The recent Intergovernmental Panel of Climate Change (IPCC) Sixth Assessment Report (AR6) (IPCC, 2021) finds that 1.5°C over pre-industrial will very likely be exceeded in the near term (2021- 2040) under the very high greenhouse gas (GHG) emission scenario (SSP5-8.5) and likely to be exceeded under the intermediate and high GHG emissions scenarios (SSP2-4.5 and SSP3-7.0). The IPCC AR6 defines 1.5°C as the time at which T0 will reach 0.65°C above the historical reference period of 1995 - 2014. The T0 between 1995 - 2014 is 0.85°C above the pre-industrial (PI) value defined as the 1850 - 1900 average in the observational record. Using 31 global models, Tebaldi et al. (2021) found that the average across models of when 1.5°C will be reached is 2028 under the SSP2-4.5 scenario (using 1995-2014 as 0.84°C rather than 0.85°C above PI), but with considerable variation across models. To simplify future model intercomparisons, we choose the time period of 2020 - 2039 (or ~ 2030 levels) as our reference period of when T0 is ~ 1.5°C above PI values and make that the target T0 in the ARISE-SAI-1.5 climate intervention simulations. We acknowledge that different climate models, with different baseline temperatures and rates of warming, might have different time periods in which they reach 1.5. Nonetheless, we recommend that the best way to achieve a meaningful and easy comparison between different models would be to use always their own model's 2020-2039 SSP2-4.5 period as a baseline over which to calculate the targets their ARISE-SAI-1.5 simulations. This way, the reference period is the same between models and the 2035 start date remains meaningful in every case.

In addition to keeping T0, the ARISE-SAI simulations aim to keep the north-south temperature gradient (T1), and equator-to-pole temperature gradient (T2) to those corresponding to the temperature target. This is achieved by utilizing a "controller" algorithm (MacMartin et al., 2014; Kravitz et al., 2017) that specifies the amount of SO_2 injection. This approach was used in GLENS and the simulations presented in Tilmes et al. (2020). The controller algorithm is freely available as described in the Code Availability section. Sulfur dioxide injections in the ARISE-SAI simulations are placed at four injection locations (15°S, 15°N, 30°S, 30°N) into one grid box at ~ 21.5 km altitude.

The injection latitudes are the same as used in GLENS and in previous studies examining the model's responses to single-point SO_2 injections (Tilmes et al., 2017; Richter et al., 2017). These four injection locations are sufficient to independently control the targets that we are trying to achieve (Kravitz et al., 2017). These four injection locations have also been demonstrated to be sufficient to produce the optical depth patterns that independently control the targets that we are trying to achieve in various versions of CESM(WACCM) (MacMartin et al., 2017; Zhang et al., 2022; MacMartin et al., 2022). The prescribed injection altitude is estimated to be achievable by existing aircraft technologies that could be adapted for climate intervention use (Bingaman et al., 2020). After each year of simulation, the algorithm calculates the global mean temperature, T0, north-south temperature gradient, T1, and equator-to-pole temperature gradient, T2, and based on the deviation from the goal, specifies the annual values of injections at the four locations for the subsequent year. T1 and T2 were defined in Kravitz et al. (2017), Equation 1.

2.4 Recommended Output

Comprehensive monthly output as well as high-frequency output for analysis of high-impact events (described in detail in the Data Records section) is needed for analysis of SCI impacts on the Earth System. Acknowledging limitations of various modeling centers, we recommended a minimum set of monthly-mean output fields in Table A1 in the Data Records section and include the full comprehensive output list that was created with the CESM2(WACCM) simulations based on input from the broader community. All model output for the simulations should be provided in NetCDF format. All variables should be in time-series format, with one variable per file. 3-dimensional atmospheric output should be on the original model levels or on standard CMIP6 levels. For monthly atmospheric output, information on aerosol microphysics (which is not a standard CMIP6 output) is also very relevant for diagnostics of the aerosols' behavior under SAI; for instance, CESM2(WACCM6) includes as standard output the mass and number concentration for all aerosol modes and the aerosol effective radius. Other modeling centers should consider providing this (model specific) information as well. In addition, higher-frequency (daily averaged, 3-hourly averaged, 3-hourly instantaneous, and 1-hourly mean) output is desired for the atmospheric model that will enable analysis of extreme events (e.g.: Tye et al. 2022). The atmospheric output at various time frequencies is described in Appendix A, Tables A2 - A5. Daily averaged output of land model variables is shown in Tables A6 and A7, whereas 6-hourly output from the land model is listed in Table A8. Tables A9 and A10 show the daily output from the ocean and sea-ice models respectively. The table captions describe which output is specific to ARISE-SAI-1.5 and the new five SSP2-4.5 CESM2(WACCM6) ensemble members, and which is common to all simulations. An online table showing all the output fields for the simulations, along with their description and units, is at: https://www.cgd.ucar.edu/ccr/strandwg/WACCM6-TSMLT-SSP245/.

2.5 Additional ARISE-SAI simulations

The ARISE-SAI-1.5 simulations described above are likely to be most relevant to policy makers and hence reproduction of the experiments in multiple models is desired. ARISE-SAI simulations are already being performed with the UKESM model. ARISE-SAI-1.0 simulations as well as ARISE-SAI-1.5-2045, with start of intervention

delayed by 10 years, are in progress with CESM2(WACCM). A subset of simulations describing these different initial conditions and targets is discussed in MacMartin et al. (2022) using a slightly more simplified version of CESM2(WACCM6).

3. ARISE-SAI-1.5 with CESM2(WACCM6)

We present here the details of implementation of ARISE-SAI-1.5 simulations in CESM2(WACCM6).

3.1 Model Description

CESM2(WACCM6) is the most comprehensive version of the NCAR whole atmosphere ESM and is described in detail in Gettelman et al., 2019; Danabasoglu et al., 2020. CESM2(WACCM6) was used to contribute climate change projection simulations to the Coupled Model Intercomparison Project Phase 6 (CMIP6) (Eyring et al., 2016). CESM2(WACCM6). CESM2(WACCM6) is a fully coupled ESM with prognostic atmosphere, land, ocean, sea-ice, land-ice, river and wave components. The atmospheric model, WACCM6, uses a finite volume dynamical core with horizontal resolution of 1.25^{o} longitude by 0.9^{o} latitude. WACCM6 includes 70 vertical levels with a model top at 4.5 $\times$ 10^{6} hPa ($\sim$ 140 km). Tropospheric physics in WACCM6 are the same as in the lower top configuration, the Community Atmosphere Model version 6 (CAM6). CESM2(WACCM6) includes a parameterization of non-orographic waves which follows Richter et al. (2010) with changes to tunable parameters described in Gettleman et al. (2019). Parameterized gravity waves are a substantial driver of the quasi-biennial oscillation (QBO) which is internally-generated in CESM2(WACCM6). CESM2(WACCM6) includes prognostic aerosols which are represented using the Modal Aerosol Model version 4 (MAM4) as described in Liu et al. (2016). This includes four modes, of which only three are used for sulfate: Aitken, Accumulation and Coarse mode. In the stratosphere, CESM(WACCM6) includes a comprehensive interactive sulfur cycle, as described for instance in Mills et al. (2016); this allows for SO_2 oxidation (with interactive OH concentration) and subsequent nucleation and coagulation of H_2SO_4 into sulfate aerosol (allowing for inter-mode transfer), which are then removed from the stratosphere through gravitational settling and large-scale circulation. A more indepth analysis of the size distribution and vertical distribution of sulfate aerosols under SO_2 injections has been performed in Visioni et al. (2022) (for single-point injections at the same latitudes and altitudes as those described in these simulations), also compared with results from other models with similar aerosol microphysics (UKESM1 and GISS), highlighting that in CESM2(WACCM6) the produced stratospheric aerosol are mainly found in the Coarse mode. CESM2(WACCM6) also includes a comprehensive chemistry module with interactive tropospheric, stratospheric, mesospheric and lower thermospheric chemistry (TSMLT) with 228 prognostic chemical species, described in detail in Gettleman et al. (2019).

The ocean model in CESM2(WACCM6) is based on the Parallel Ocean Program version 2 (POP2; Smith et al., 2010; Danabasoglu et al., 2012; Danabasoglu et al., 2020). The horizontal resolution of POP2 is uniform in the zonal direction (1.125^{o}) and varies from 0.64° (occurring in the Northern Hemisphere) to 0.27° at the Equator. The ocean biogeochemistry is represented using the Marine Biogeochemistry Library (MARBL), which is an updated

implementation of the Biochemistry Elemental Cycle (Moore et al., 2002; 2004; 2013). CESM2 uses version 3.14 of the NOAA WaveWatch-III ocean surface wave prediction model (Tolman, 2009). Sea-ice in CESM2(WACCM6) is represented using CICE version 5.1.2 (CICE5; Hunke et al., 2015) and uses the same horizontal grid as POP2.

CESM2(WACCM6) uses the Community Land Model version 5 (CLM5) (Lawrence et al., 2019). CLM5 includes a global crop model that treats planting, harvest, grain fill, and grain yields for six crop types (Levis et al., 2018), a new fire model (Li et al., 2013; Li and Lawrence, 2017), multiple urban classes and an updated urban energy model (Oleson & Feddema, 2019), and improved representation of plant dynamics. The river transport model used is the Model for Scale Adaptive River Transport (MOSART; H. Y. Li et al., 2013).

3.2 Reference simulations

A 5-member reference ensemble with CESM2(WACCM6) and the SSP2-4.5 scenario was carried out as part of the CMIP6 project for years 2015 - 2100. Surface temperature evolution and equilibrium climate sensitivity in these simulations are described in detail in Meehl et al. (2020). We carried out an additional 5-member ensemble of these simulations from years 2015 - 2069 with augmented high-frequency output for high-impact event analysis, as well as additional output for the land model to match the SCI simulations. The additional 5-member ensemble was branched from the three existing historical CESM2(WACCM6) simulations in the same manner as the first 5-member ensemble, but with an addition of small temperature perturbations for each ensemble member ([6, 7, 8, 9, 10] $x10^{-14}$ K, respectively), at the first model timestep. CESM2 ranks highly against other CMIP6 models in the ability to represent large scale circulations and key features of tropospheric climate over the historical time period (e.g.: Simpson et al., 2020; Duviver et al., 2020; Coburn and Pryor 2021).

3.3 ARISE-SAI-1.5 Simulations

In CESM2(WACCM6) SO_2 injections were placed at 180° longitude and bounded by two pressure interfaces: 47.1 hPa and 39.3 hPa (approximate geometric altitude at gridbox midpoint of 21.6 km). Based on the 2020 - 2039 mean of the SSP2-4.5 simulations with CESM2(WACCM6), the surface temperature targets for the ARISE-SAI-1.5 ensemble for T0, T1, and T2 are 288.64 K, 0.8767 K, and -5.89 K, respectively. As noted in section 2.3, we recommend that T0, T1, and T2 targets for other models reproducing ARISE-SAI-1.5 simulations are based on the 2020 – 2039 average from their SSP2-4.5 simulations.

The first five members of ARISE-SAI-1.5 simulations were initialized in 2035 from the first five members (001 to 005) of the SSP2-4.5 simulations carried out with CESM2(WACCM6); hence, all had different initial ocean, sea-ice, land, and atmospheric initial conditions on January 1, 2035. Similarly to the SSP2-4.5 simulations, subsequent ensemble members (006 through 010) were initialized from the same initial conditions as members 001 through 005, respectively, with an addition of a small temperature perturbation to the atmospheric initial condition to create ensemble spread.

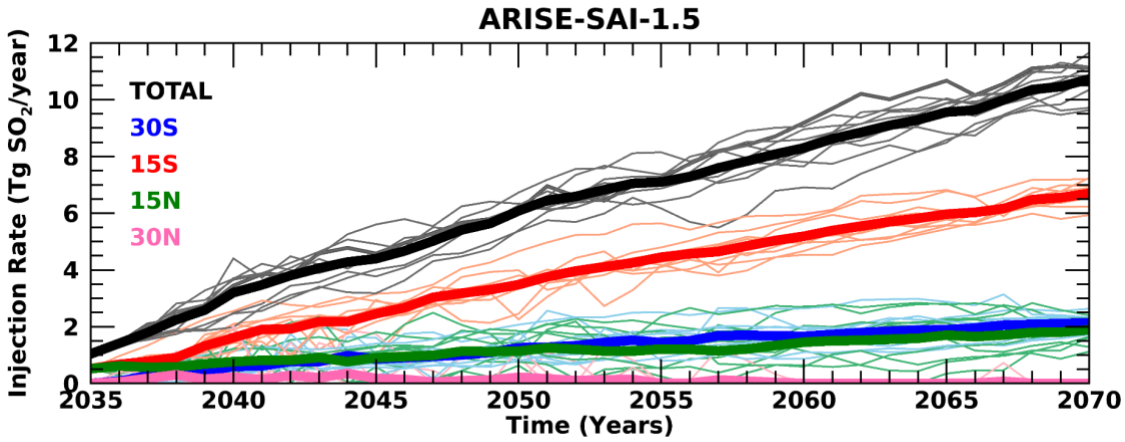

Figure 1: SO_2 injection rate as a function of time in ARISE-SAI-1.5 simulations at 30ºS (blue), 15ºS (red), 15ºN (green), 30ºN (pink), and total (black). Thin lighter colored lines represent individual ensemble members, whereas thick lines show the 10-member ensemble mean.

The amount of SO_2 injection in the ARISE-SAI-1.5 simulations chosen by the controller algorithm is shown in Figure 1. The majority of SO_2 is injected at 15ºS, with an approximate linear increase from 0.5 Tg SO_2 per year in 2035 to 6 Tg SO_2 per year in 2069. SO_2 injections at 30ºS and 15ºN are about ⅓ of that injected at 15ºS. Throughout all the ARISE-SAI-1.5 simulations, the amount of SO_2 injection at 30ºN is very small, less than 0.5 Tg SO_2 per year, diminishing to nearly zero by the end of the simulations. The distribution of SO_2 across the four injection latitudes in ARISE-SAI-1.5 is very different from that in GLENS (Tilmes et al., 2018) despite having the same goals for the controller. In GLENS, the majority of SO_2 was injected at 30ºS and 30ºN, with a significant amount at 15ºN, and almost none at 15ºS; that is, GLENS required more injection in the Northern Hemisphere than the Southern in order to maintain the interhemispheric temperature gradient T1, whereas ARISE-SAI-1.5 requires more injection in the Southern Hemisphere to maintain T1. GLENS also required more SO_2 injection at 30ºN/30ºS to maintain T2 than is required in ARISE-SAI-1.5. It is unclear at this time how much of this difference is a result of the different model version and how much is a result of changes in the forcing between RCP8.5 and SSP2-4.5.

4 Initial Results

One of the intents of ARISE-SAI simulations is to provide the broader community a data set for examining various impacts of SCI on the multiple components of the Earth system. Below we present basic diagnostics that verify that the SO_2 injections and controller are working as intended, and we describe how well the temperature targets are being met in CESM2(WACCM6). Detailed analysis of the simulations is left for future work.

4.1 Stratospheric Aerosols

Injection of sulfur dioxide into the stratosphere results in the formation of sulfate aerosols, which are transported by the stratospheric Brewer-Dobson circulation (Andrews et al., 1987; Tilmes et al., 2017). The dominance of SO_2 injections at 15ºS in ARISE-SAI-1.5 results in a stratospheric sulfate (SO_4) increase that primarily occurs in the southern hemisphere, with the majority of SO_4 concentrated near the primary injection location (Figure 2a, 2b). Averaged over the 2035 - 2054 period, there is a peak SO_4 increase of 25 mg-S/kg air (Fig 2a) relative to the 2020 - 2039 mean, and averaged over 2050 - 2069 an SO_4 increase of 48 mg-S/kg air is found near 15ºS, 40 hPa (Fig 2b). The zonally averaged latitudinal distribution of the increase in the column of SO_4 is shown in Figures 2c, d; both figures show the strong hemispheric asymmetry, and also a double peak at around 15ºS and one near 50ºS. The peak near 15ºS is due to the predominant location of the injection, and matches the peak in concentration, the latter is due to the largest vertical stratospheric layer over which SO_4 is spread out (between 10 and 22 km) compared to the layer in the tropical stratosphere (between 18 and 26 km). Integrated over 20-year periods of ARISE-SAI-1.5 simulations, there is little difference in the latitudinal distribution of column SO_4 between the various ensemble members, but amplitude differences of up to 15% exist (not shown), reflecting variability in the amount of SO_2 injection at each location and small differences in the stratospheric circulation.

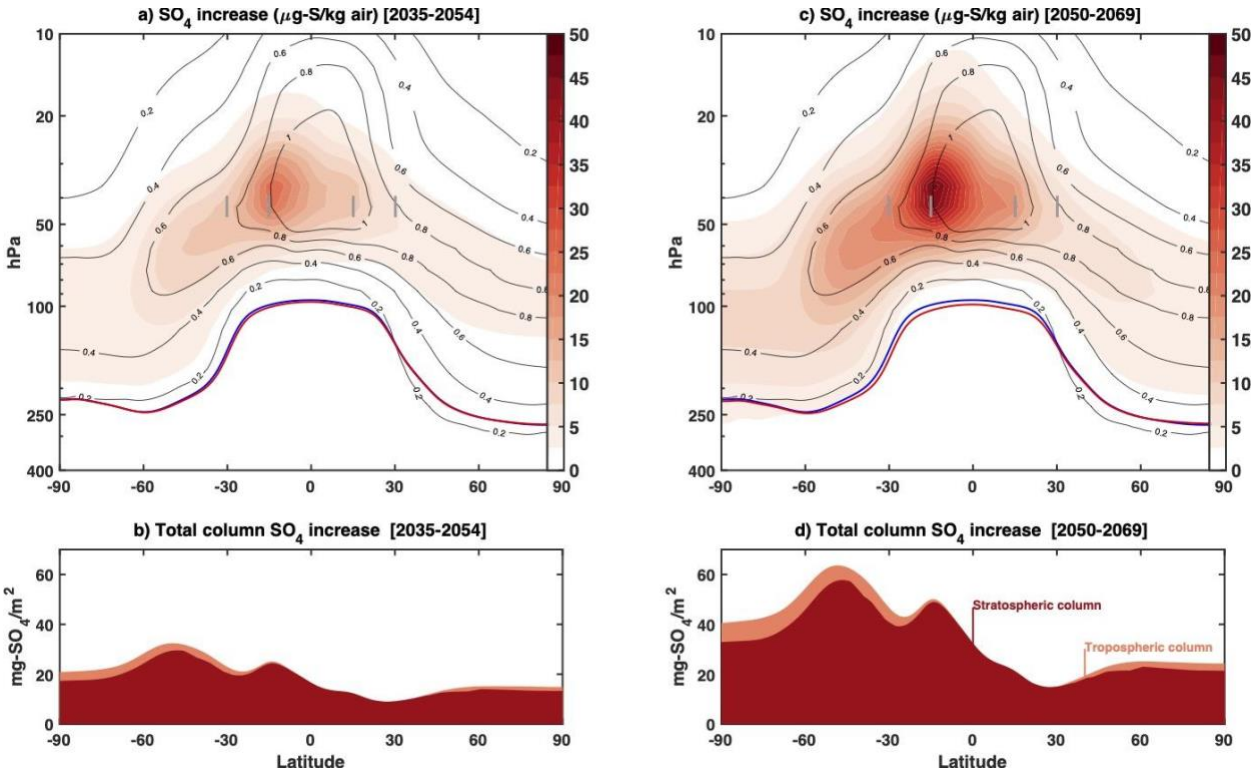

Figure 2: Zonal mean stratospheric SO_4 concentration increase (in µg-S/kg of air) in (a) 2035-2054 and (c) 2050-2069 relative to the 2020 - 2039 mean. Black contour lines show the background concentration in 2020-2039. Blue line shows the annual mean tropopause height in the control period; the red line shows the annual mean tropopause height in the ARISE simulation in 2035-2054 and 2050-2069, respectively. Gray shadings indicate the grid-boxes

where SO_2 is injected. Zonal mean total increase in the column burden of sulfate (in mg-SO_4/m^2) for (b) 2035 - 2054 and (d) 2050 - 2069. The contribution to the column increase is shown in dark red, for the fraction located in the stratosphere, and in orange for the fraction located in the troposphere.

4.2 Meeting temperature targets

Global mean surface temperature, the inter-hemispheric temperature gradient, and equator-to-pole temperature gradients for the SSP2-4.5 and ARISE-SAI-1.5 simulations are shown in Figure 3. There is a notable difference in behavior of T1 and T2 in the SSP2-4.5 simulations as compared to the RCP8.5 simulations with CESM1(WACCM) (not shown). In the CESM1(WACCM) simulations with RCP8.5, T1 and T2 were increasing steadily with time of simulation, reaching a change in T1 of nearly 0.45 K, and a T2 change of 0.3 K by 2070 relative to ~ 2020 - 2039 mean (Tilmes et al. 2018). In contrast, T1 and T2 in the SSP2-4.5 simulation are increasing much more slowly, less than 0.05 K for T1 and less than 0.1 K for T2 between the reference period (2020-2039) and 2070. The more moderate (SSP2-4.5) emission scenario used in the CESM2(WACCM6) control simulations partially explains the slower increase of T1 and T2 with time, however not all. Simulations with CESM2(WACCM6) and SSP5-8.5 scenarios also show a much slower increase of T1 and T2 as compared to CESM1(WACCM) with RCP8.5. Differing modeling physics, in particular cloud feedbacks, between CESM1 and CESM2 are key differences that could lead to the differences in projected spatial patterns of surface warming between the two model configurations, as well as changes in the Atlantic Meridional Overturning Circulation as discussed in Tilmes et al. (2020). Additional simulations with CESM2 and RCP emissions have been performed to understand the relative role of differences in forcing and differences in model physics on projected spatial patterns of global mean temperature and other variables between CESM1 and CESM2. A detailed discussion of the reasons behind the model dependence in injection strategy in GLENS, CESM1(WACCM) and ARISE-SAI-1.5, CESM2(WACCM6) simulations can be found in Fasullo and Richter (2022). They show that the main contributors to the differences are: rapid adjustment of clouds and rainfall to elevated levels of carbon dioxide, dynamical responses in the Atlantic Meridional Overturning Circulation (AMOC) and differences in future climate forcing scenarios.

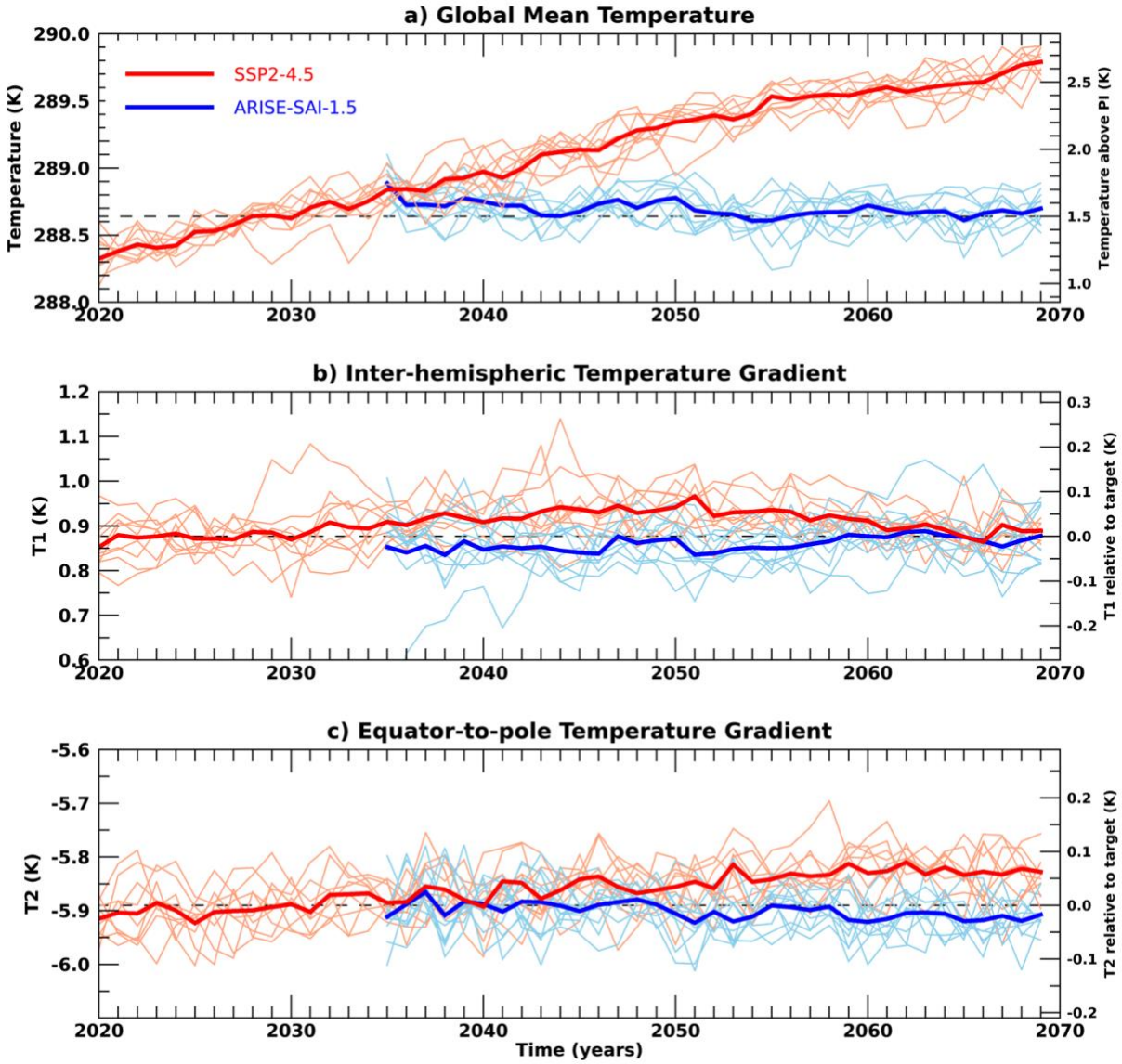

Figure 3: Global mean a) surface temperature, b) inter-hemispheric temperature gradient, T1, and c) equator-to-pole temperature gradient, T2, for SSP2-4.5 (red) and ARISE-SAI-1.5 (blue) simulations. Thin lines represent individual ensemble members, whereas the thick lines show the ensemble mean.

The differences between the projected surface temperature patterns in CESM2 as compared to CESM1 have implications for climate intervention. Since the changes in T1 and T2 targets differ between the CESM1(WACCM) and CESM2(WACCM6) future simulations, the controller selects different SO_2 injection locations to best counteract these changes. Injections needed to offset increasing T1 and T2 in CESM1(WACCM) required primarily injections at 30°S and 30°N, whereas a small change in T1 and T2 relative to the 2020 - 2039 period in CESM2(WACCM6), SSP2-4.5 requires injections primarily at 30°S. The SO_2 injections applied in ARISE-SAI-1.5 do a very good job at keeping the global mean temperature, T1 and T2 at the target levels. This is demonstrated by the blue lines in Figure 2. There

is a fair amount of variability among the individual ensemble members (thin light blue lines) in their ability to meet the global mean, T1 and T2 targets, however the ensemble mean (thick blue line) shows very good agreement between these variables and their target values.

4.3 Surface temperature and precipitation

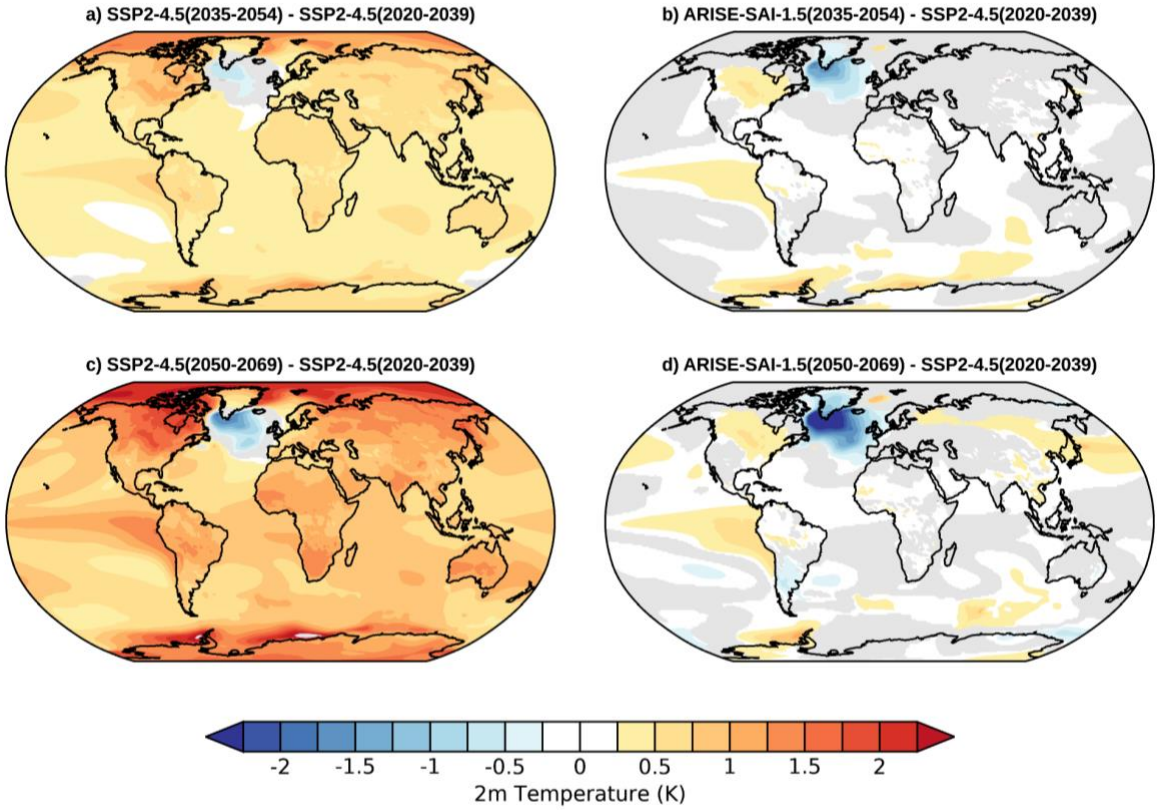

Figure 4: Ensemble and annual mean surface (2m) temperature differences between a) SSP2-4.5 (2035-2054) and SSP2-4.5 (2020-2039), b) ARISE-SAI-1.5 (2035-2054) and SSP2-4.5 (2020-2039), c) SSP2-4.5 (2050-2069) and SSP2-4.5 (2020-2039), and d) ARISE-SAI-1.5 (2050-2069) and SSP2-4.5 (2020-2039). Gray shading indicates regions where the differences are not statistically significant at the 95% level using a two-sided Student's t test.

Figure 4 shows the ensemble and annual mean surface temperature changes for two time periods, 2035 - 2054 and 2050 - 2069, during the SSP2-4.5 and ARISE-SAI-1.5 simulations relative to the 2020 - 2039 period. Fig 4 a, c show the steady increase in surface temperature with time over the majority of the globe, with the largest warming occurring in the Northern Hemisphere high latitudes. The North Atlantic is the only region of the globe that is cooling in the 21st century. This "warming hole" in the North Atlantic is a feature of several of the recent generation Earth system models and is attributed to the AMOC (Drijfhout et al. 2012, Chemke et al. 2020, Keil et al. 2020). Specifically, in a warming climate with a reduction in the deep water formation, the AMOC weakens. This results in less heat transport

into the Northern North Atlantic, producing cooler temperatures that oppose the anticipated effects of global warming. Figures 4b and 4d demonstrate the success of the SAI strategy in keeping the global temperatures near the 2020 - 2039 average, or at ~ 1.5 K above pre-industrial values. In ARISE-SAI-1.5, near surface annual mean temperature throughout the entire simulation is within 0.5 K of that goal over the majority of the globe. The largest exception to that is the North Atlantic warming hole, where surface temperatures remain cooler relative to the northern North Atlantic than in the present day; while AMOC strength is partially recovered under SAI relative to SSP2-4.5, it is not fully restored back to present-day conditions. In addition, in the ensemble mean, ARISE-SAI-1.5 simulations show residual warming over North America, as well as over Eastern South Pacific Ocean (off the coast of South America), and in parts of Antarctica as compared to the 2020 - 2039 period. Residual changes relative to the target period from the application of SAI are expected, as SAI can not perfectly reverse the effects of increasing greenhouse gases.

The precipitation changes in SSP2-4.5 and ARISE-SAI-1.5 simulations for the same time periods examined for surface temperature changes are shown in Figures 5 and 6. Consistent with prior similar studies, SSP2-4.5 simulations show primarily an increase of precipitation in a warming climate, with the largest increases along the Equatorial Pacific Ocean, and a strong drying region northward of that (Figs 5, 6a,c). In ARISE-SAI-1.5, consistent with previous studies (Kravitz et al., 2017; Lee et al. 2020), restoring global mean temperature is associated with an overall decrease in annual mean precipitation (Fig 5), however regionally both increases and decreases occur. In ARISE-SAI-1.5, the increased precipitation across the Equatorial Pacific seen in SSP2-4.5 decreases in magnitude, but is still a persistent feature. ARISE-SAI-1.5 also shows drying north and south of that region as well as intensified drying over Northern South America, South Africa, Indian Ocean south of the Equator and northernmost Australia. The Indian Ocean north of the Equator and India are projected to be wetter in ARISE-SAI-1.5 as compared to the 2020 - 2039 period of SSP2-4.5.

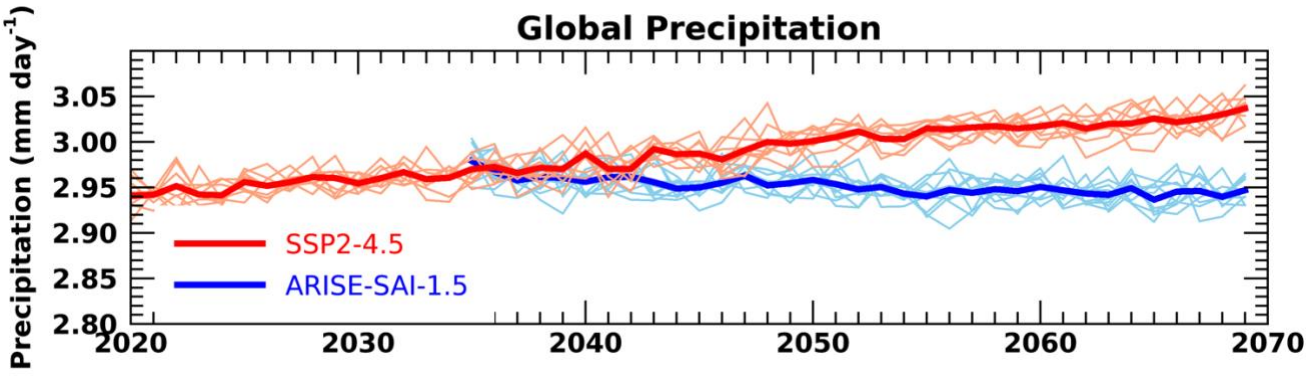

Figure 5: Same as Figure 3a but for precipitation.

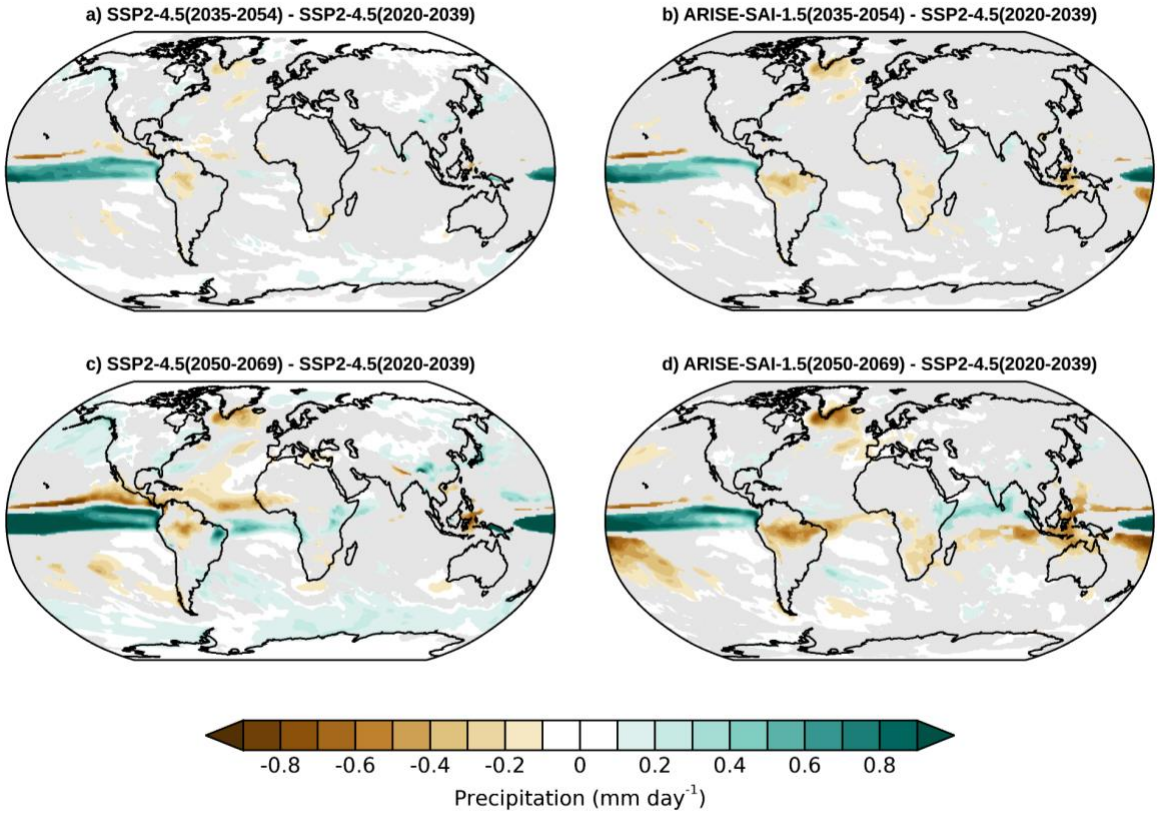

Figure 6: Same as Figure 4 but for annual mean precipitation.

5 Conclusions

We have described here a detailed new modeling protocol and the first set of simulations of Assessing Responses and Impacts of Solar climate intervention on the Earth system with Stratospheric Aerosol Injection (ARISE-SAI), for studies of impacts of climate intervention using stratospheric aerosols. We have carried out the ARISE-SAI-1.5 simulations utilizing CESM2(WACCM6) and provided extensive output for community analysis. The protocol for simulations described here can be easily implemented in other Earth system models with similar capabilities; furthermore, the protocol can easily be adapted to explore different climate intervention scenarios considering other climate targets, such as different global mean cooling targets, and in the future extended to other types of climate intervention, such as marine cloud brightening. The SAI injection strategy defined by the protocol builds on the approach used in GLENS that was carried out with CESM1(WACCM), but uses a more moderate background emissions scenario, a start date of 2035 rather than 2020, and a target temperature of 1.5ºC over pre-industrial following the AR6 definition; the set of simulations presented here also uses a newer version of CESM, which is the same as used for CMIP6 (Gettelman et al., 2019). In these new simulations, the SO_2 injections required to keep the global mean temperature, interhemispheric temperature gradient, and pole-to-pole temperature gradient at the target level in ARISE-SAI-1.5 are needed primarily at 15ºS, in contrast to GLENS which utilized SO_2 injections primarily

at 30ºN and 30ºS. The reasons for these differences are currently being investigated in detail, and it highlights the need to reproduce such experiments with other climate models to understand their sources. Surface climate in ARISE-SAI-1.5 is very similar to that during the reference period (2020 - 2039), however residual changes still remain, in particular in the North Atlantic, where surface temperature is cooler than in the reference period. The robustness of these projected regional residuals in other climate models, or under different climate targets, would also be of extreme interest. Consistent with prior studies, global mean precipitation in ARISE-SAI-1.5 is smaller than during the reference period.

The output for the ARISE-SAI-1.5 simulations is extensive and includes variables from multiple Earth system components enabling the community analysis of changes in many variables that are crucial to making decisions about the implementation of SCI including weather and climate extremes, crops, ozone changes, etc. To enable broad access to the data, output from the ARISE-SAI-1.5 simulations is available on the Amazon Web Services Open Data portal.

Appendix A

Variable Name	**Description**
AEROD_v	Total Aerosol Optical Depth in visible band
AODVIS	Aerosol optical depth 550 nm, day only
BURDENSO4dn	Sulfate aerosol burden, day night
CLDHGH	Vertically-integrated high cloud
CLDLOW	Vertically-integrated low cloud
CLDMED	Vertically-integrated mid-level cloud
CLDTOT	Vertically-integrated total cloud
CLOUD	Cloud fraction
dgnumwet1	Aerosol mode (accumulation) wet diameter
dgnumwet2	Aerosol mode (Aitken) wet diameter
dgnumwet3	Aerosol mode (coarse) wet diameter
DTCOND	T tendency - moist processes
FLDS	Downwelling longwave flux at surface
FLDSC	Clearsky Downwelling longwave flux at surface
FLNR	Net longwave flux at tropopause

FLNS	Net longwave flux at surface
FLNSC	Clearsky net longwave flux at surface
FLNT	Net longwave flux at top of model
FLNTC	Clearsky net longwave flux at top of model
FLUT	Upwelling longwave flux at top of model
FLUTC	Clearsky upwelling longwave flux at top of model
FSDS	Downwelling solar flux at surface
FSDSC	Clearsky downwelling solar flux at surface
FSNR	Net solar flux at tropopause
FSNS	Net solar flux at surface
FSNSC	Clearsky net solar flux at surface
FSNTOA	Net solar flux at top of atmosphere
FSNTOAC	Clearsky net solar flux at top of atmosphere
FSNT	Net solar flux at top of model
FSNTC	Clearsky net solar flux at top of model
LWCF	Longwave cloud forcing
H2O	Water vapor concentration
ICEFRAC	Fraction of sfc area covered by sea-ice
num_a1	Aerosol mode (accumulation) number concentration
num_a2	Aerosol mode (Aitken) number concentration
num_a3	Aerosol mode (coarse) number concentration
O3	Ozone concentration
O3_Loss	Ozone reaction rate group
O3_Prod	Ozone reaction rate group
MSKtem	Transformed Eulerian Mean diagnostics mask
OMEGA	Vertical velocity (pressure)
PBLH	PBL height
PHIS	Surface geopotential

PRECC	Convective precipitation rate
PRECT	Total (convective and large-scale) precipitation rate
PRECTMX	Maximum (convective and large-scale) precipitation rate
PS	Surface pressure
PSL	Sea level pressure
Q	Specific humidity
QRL	Longwave heating rate
QRL_TOT	Merged LW heating: QRL+QRLNLTE
QRS	Solar heating rate
QRS_TOT	Merged SW heating:
QSNOW	Diagnostic grid-mean snow mixing ratio
RELHUM	Relative humidity
REFF_AERO	Aerosol effective radius
RHREFHT	Reference height relative humidity
SO2	Sulfur dioxide concentration
so4_a1	so4_a1 (accumulation) concentration
so4_a2	so4_a2 (Aitken) concentration
so4_a3	so4_a3 (coarse) concentration
SST	sea surface temperature
SWCF	Shortwave cloud forcing
T	Temperature
TREFHT	Reference height temperature
TREFHTMN**	Minimum reference height temperature
TREFHTMX**	Maximum reference height temperature
TS	Surface temperature (radiative)
TROP_P	Tropopause Pressure
TROP_T	Tropopause Temperature
TSMN	Minimum surface temperature

TSMX	Minimum surface temperature
U	Zonal wind
U10	10m wind speed
V	Meridional wind
Z3	Geopotential Height (above sea level)
Z500	Geopotential height at 500 hPa pressure surface

Table A1: Minimum recommended monthly mean output for ARISE-SAI simulations and corresponding reference simulations.

Variable Name	**Description**
ACTNL	Average Cloud Top droplet number
ACTREL	Average Cloud Top droplet effective radius
bc_a4_SRF*	Black carbon in additional mode in bottom layer
BURDENBCdn	Black carbon aerosol burden, day night
BURDENDUSTdn	Dust aerosol burden, day night
BURDENPOMdn	Particulate organic matter aerosol burden, day night
BURDENSEASALTdn	Seasalt aerosol burden, day night
BURDENSO4dn	Sulfate aerosol burden, day night
BURDENSOAdn	SOA aerosol burden, day night
BUTGWSPEC	Zonal wind tendency from convective gravity waves
CDNUMC	Vertically-integrated droplet concentration
CLDICE	Grid box averaged cloud ice amount
CLDLIQ	Grid box averaged cloud liquid amount
CLDTOT	Vertically-integrated total cloud
CLOUD	Cloud fraction
CMFMC	Moist convection (deep+shallow) mass flux
CMFMCDZM	Convection mass flux from ZM deep
dst_a1*	Dust concentration in accumulation mode

dst_a2*	Dust concentration in Aitken mode
dst_a3*	Dust concentration in coarse mode
dst_a2_SRF*	Aitken mode dust in bottom layer
FCTL	Fractional occurrence of cloud top liquid
FLDS	Downwelling longwave flux at surface
FLDSC	Clearsky Downwelling longwave flux at surface
FLNR	Net longwave flux at tropopause
FLNS	Net longwave flux at surface
FLNSC	Clearsky net longwave flux at surface
FLNT	Net longwave flux at top of model
FLNTC	Clearsky net longwave flux at top of model
FLUT	Upwelling longwave flux at top of model
FLUTC	Clearsky upwelling longwave flux at top of model
FSDS	Downwelling solar flux at surface
FSDSC	Clearsky downwelling solar flux at surface
FSNR	Net solar flux at tropopause
FSNS	Net solar flux at surface
FSNSC	Clearsky net solar flux at surface
FSNTOA	Net solar flux at top of atmosphere
FSNTOAC	Clearsky net solar flux at top of atmosphere
LHFLX	Surface latent heat flux
MASS	mass of grid box
O3	Ozone
MSKtem	Transformed Eulerian Mean diagnostics mask
OMEGA	Vertical velocity (pressure)
OMEGA500	Vertical velocity at 500 hPa
PBLH	Planetary boundary layer height
PDELDRY	Dry pressure difference between levels

PHIS	Surface geopotential
PM25_SRF	PM2.5 in the bottom layer
pom_a4_SRF*	Particulate organic matter in additional mode in bottom layer
PRECC	Convective precipitation rate
PRECT	Total (convective and large-scale) precipitation rate
PRECTMX	Maximum (convective and large-scale) precipitation rate
PS	Surface pressure
PSL	Sea level pressure
Q	Specific humidity
QREFHT	Reference height humidity
QSNOW	Diagnostic grid-mean snow mixing ratio
RELHUM	Relative humidity
RHREFHT	Reference height relative humidity
SFso4_a1*	surface flux of SO_4 in accumulation mode
SFso4_a2*	surface flux of SO_4 in Aitken mode
SFbc_a4*	Surface flux of black carbon in additional mode
SFpom_a4*	Particulate organic matter in additional mode
SFdst_a1*	Surface flux of dust in accumulation mode
SFdst_a2*	Surface flux of dust in Aitken mode
SFdst_a3*	Surface flux of dust in coarse mode
SHFLX	Surface sensible heat flux
SO2	Sulfur dioxide concentration
SOLIN	Solar insolation
SOLLD	Solar downward near infrared diffuse to surface
SOLSD	Solar downward visible diffuse to surface
T	Temperature
T500, T700, T850	Temperature at 500, 700 and 850 hPa respectively
TAUBLJX	Zonal integrated drag from Beljaars SGO

TAUBLJY	Meridional integrated drag from Beljaars SGO
TAUGWX	Zonal gravity wave surface stress
TAUGWY	Meridional gravity wave surface stress
TAUX	Zonal surface stress
TAUY	Meridional surface stress
TGCLDIWP	Total grid-box cloud ice water path
THzm	Zonal-Mean potential temperature defined on ilevels
TGCLDLWP	Total grid-box cloud liquid water path
TMQ	Total (vertically integrated) precipitable water
TREFHT	Reference height temperature
TREFHTMN**	Minimum reference height temperature
TREFHTMX**	Maximum reference height temperature
TS	Surface temperature (radiative)
TSMN	Minimum surface temperature
TSMX	Minimum surface temperature
U	Zonal wind
U10	10m wind speed
UTGWORO	U tendency - orographic gravity wave drag
UTGWSPEC	U tendency - non-orographic gravity wave drag
UVzm	Meridional flux of zonal momentum: 3D zonal mean
UWzm	Vertical flux of zonal momentum: 3D zonal mean
Uzm	Zonal mean zonal wind defined on ilevels
V	Meridional wind
VTHzm	Meridional Heat Flux: 3D zonal mean
Vzm	Zonal mean meridional wind defined on ilevels
Wzm	Zonal mean vertical wind defined on ilevels
Z3	Geopotential Height (above sea level)
Z500	Geopotential height at 500 hPa pressure surface

412

Table A2: Available daily averaged output from the atmospheric model in ARISE-SAI-1.5 simulations and SSP2-4.5 CESM2(WACCM6) simulations. Variables marked with a '*' are not available from the first five members of CESM2(WACCM6) SSP2-4.5 simulations. **indicates variables that are available (but erroneous) in the first five members of CESM2(WACCM6) SSP2-4.5 simulations. Variables in bold are used to calculate extremes indices such as those presented in Tye et al. (2022).

Name of Variable(s)	**Variable Description**
CAPE	Convective available potential energy
CIN	Convective inhibition
CLDLOW	Vertically-integrated low cloud
FLUT	Upwelling longwave flux at top of model
PRECT	Total (convective and large-scale) precipitation rate
PRECC	Convective precipitation rate
PRECSC	Convective snow rate (water equivalent)
PRECSL	Large-scale snow rate (water equivalent)
PSL	Sea level pressure
Q200, Q500, Q700, Q850, Q925	Specific humidity at 200, 500, 700, 850 and 925 hPa respectively
T200, T300, T500, T700, T850, T925	Temperature at 200, 300, 500, 700, 850 and 925 hPa respectively
TMQ	Total (vertically integrated) precipitable water
U200, U300, U500, U700, U850, U925	Zonal wind at 200, 300, 500, 700, 850 and 925 hPa respectively
V200, V300, V500, V700, V850, V925	Meridional wind at 200, 300, 500, 700, 850 and 925 hPa respectively
Z200, Z500, Z700, Z850, Z925	Geopotential height at 200, 500, 700, 850 and 925 hPa respectively

Table A3: 3-hourly averaged output from the atmospheric model in ARISE-SAI-1.5 simulations and additional five SSP2-4.5 CESM2(WACCM6) simulations. None of the above output is contained in the first five ensemble members of CESM2(WACCM6) SSP2-4.5 simulations.

IVT	Integrated water vapor transport
PS	Surface Pressure
Q*	Specific humidity
T*	Temperature
TS	Surface temperature (radiative)
PSL	Sea level pressure
RELHUM*	Relative humidity
TMQ	Total (vertically integrated) precipitable water
U*	Zonal wind
U10	10m wind speed
uIVT	Zonal water vapor transport
vIVT	Meridional water vapor transport
V*	Meridional wind
Z3*	Geopotential Height

Table A4: 3-hourly instantaneous output from the atmospheric model in ARISE-SAI-1.5 simulations and additional five SSP2-4.5 CESM2(WACCM6) simulations. For the variables marked with a '*', only the bottom-most 22 levels were retained, hence levels for those variables range from 1000 to 103 hPa. None of the above output is contained in the first five ensemble members of CESM2(WACCM6) SSP2-4.5 simulations.

Name of Variable	Variable Description
NO2_SRF	NO2 in bottom layer
O3_SRF	O3 in bottom layer
PM25_SRF	PM2.5 at the surface
PRECC	Convective precipitation rate
PRECT	Total (convective and large-scale) precipitation rate
TS	Surface temperature (radiative)

Table A5: 1-hourly instantaneous output from the atmospheric model in ARISE-SAI-1.5 simulations and additional five SSP2-4.5 CESM2(WACCM6) simulations. None of the above output is contained in the first five ensemble members of CESM2(WACCM6) SSP2-4.5 simulations.

Variable Name	Description
AR	Autotrophic respiration
COL_FIRE_CLOSS	Total column-level fire C loss
CPHASE	Crop phenology phase
DSTDEP	Total dust deposition
DSTFLXT	Total surface dust emission
DWT_CONV_CFLUX_PATCH	Patch-level conversion C flux
DWT_SLASH_CFLUX	Slash C flux to litter and CWD due to land use
DWT_WOOD_PRODUCTC_GAIN_PATCH	Patch-level landcover change-driven addition to wood product pools
EFLX_LH_TOT	Total latent heat flux
FGR	Heat flux into soil/snow including snow melt and lake / snow light transmission
FIRA	Net infrared (longwave) radiation
FIRE	Emitted infrared (longwave) radiation
FROOTC	Fine root carbon

FSH	Sensible heat not including correction for land use change and rain/snow conversion
FSR	Reflected solar radiation
GDDHARV	Growing degree days needed to harvest
GDDPLANT	Accumulated growing degree days past planting date for crop
GPP	Gross primary production
GRAINC_TO_FOOD	Grain carbon to food
H2OSNO	Snow depth (liquid water)
HR	Total heterotrophic respiration
HTOP	Canopy top
NPP	Net primary production
Q2M	2m specific humidity
QDRAI	Sub-surface drainage
QDRAI_XS	Saturation excess drainage
QIRRIG	Water added through irrigation
QOVER	Surface runoff
QRUNOFF	Total liquid runoff
QSNOMELT	Snow melt rate
QSOIL	Ground evaporation
QTOPSOIL	Water input to surface
QVEGE	Canopy evaporation
QVEGT	Canopy transpiration
RH2M	2m relative humidity
SLASH_HARVESTC	Slash harvest carbon
SNOWDP	Gridcell mean snow height
SOILWATER_10CM	Soil liquid water + ice in top 10cm of soil
TG	Ground temperature
TLAI	Total projected leaf area index
TOTSOILLICE	Vertically summed soil ice

TOTSOILLIQ	Vertically summed soil liquid water
TREFMNAV	Daily minimum of average 2-m temperature
TREFMXAV	Daily maximum of average 2-m temperature
TSA	2m air temperature
TSKIN	Skin temperature
TSOI_10CM	Soil temperature in top 10cm of soil
TV	Vegetation temperature
TWS	Total water storage
U10	10-m wind
U10_DUST	10-m wind for dust model
URBAN_HEAT	Urban heating flux
WASTEHEAT	Sensible heat flux from heating/cooling sources of urban waste heat
WOOD_HARVESTC	Wood harvest carbon

438

439 **Table A6:** Available daily averaged output from the land model at landunit-level in ARISE-SAI-1.5 simulations and
440 additional five SSP2-4.5 CESM2(WACCM6) simulations. None of the above output is contained in the first five
441 ensemble members of CESM2(WACCM6) SSP2-4.5 simulations.

442

CPHASE	Crop phenology phase
CROPPROD1C	1-yr grain product carbon
CWDC_vr	Coarse woody debris carbon, vertically resolved)
CWDN_vr	Coarse woody debris nitrogen (vertically resolved)
EFLX_LH_TOT	Total latent heat flux
FGR	Heat flux into soil/snow including snow melt and lake / snow light transmission
FPSN	Photosynthesis
FROOTC	Fine root carbon
FSH	Sensible heat not including correction for land use change and rain/snow conversion
FSNO_ICE	Fraction of ground covered by snow

GDDHARV	Growing degree days needed to harvest
GDDPLANT	Accumulated growing degree days past planting date for crop
GPP	Gross primary production
GRAINC	Grain carbon
H2OSOI	Volumetric soil water
HTOP	Canopy top
LEAFC	Leaf carbon
LEAFN	Leaf Nitrogen
LITR1C_vr, LITR2C_vr, LITR3C_vr	Amount of carbon in litter in different decomposition pools, vertically resolved
LITR1N_vr, LITR2N_vr, LITR3N_vr	Amount of nitrogen in litter in different decomposition pools, vertically resolved
LIVESTEMC	Live stem carbon
PCT_CFT	% of each crop on the crop landunit
PCT_GLC_MEC	% of each GLC elevation class on the glc_mec landunit
PCT_LANDUNIT	% of each landunit on grid cell
PCT_NAT_PFT	% of each PFT on the natural vegetation (i.e., soil) landunit
QICE_FORC	Surface mass balance of glaciated grid cells forcing sent to the glacier model
QIRRIG	Water added through irrigation
RAIN	Atmospheric rain, after rain/snow repartitioning based on temperature
Rnet	Net radiation
SMINN	Soil mineral N
SMP	Soil matric potential
SOILC_vr	SOIL C (vertically resolved)
SOILN_vr	SOIL N (vertically resolved)
TLAI	Total projected leaf area index
TOPO_FORC	Topographic height sent to glacier model

TOTLITC	Total litter carbon
TOTSOMC	Total soil organic matter carbon
TOTVEGC	Total vegetation carbon, excluding cpool
TOT_WOODPRODC	Total wood product carbon
TREFMNAV	Daily minimum of average 2-m temperature
TREFMXAV	Daily maximum of average 2-m temperature
TSA	2m air temperature
TSAI	Skin temperature
TSRF_FORC	Surface temperature sent to glacier model
TV	Vegetation temperature

Table A7: Available daily averaged output from the land model at gridcell-level in ARISE-SAI-1.5 simulations and additional five SSP2-4.5 CESM2(WACCM6) simulations. None of the above output is contained in the first five ensemble members of CESM2(WACCM6) SSP2-4.5 simulations.

Name of Variable	Variable Description
EFLX_LH_TOT	Total latent heat flux
FSH	Sensible heat not including correction for land use change and rain/snow conversion
H2OSNO	Snow depth (liquid water)
H2OSOI	Volumetric soil water
QDRAI	Sub-surface drainage
QDRAI_XS	Saturation excess drainage
QOVER	Surface runoff
QRUNOFF	Total liquid runoff
QSNOMELT	Snow melt rate
QSOIL	Ground evaporation
QTOPSOIL	Water input to surface
QVEGE	Canopy evaporation
QVEGT	Canopy transpiration
SOILICE	Soil ice
SOILLIQ	Soil liquid water
SOILWATER_10CM	Soil liquid water and ice in top 10cm of soil
TOTSOILICE	Vertically summed soil cice
TOTSOILLIQ	Vertically summed soil liquid water
TWS	Total water storage

Table A8: 6-hourly averaged output from the land model in ARISE-SAI-1.5 simulations and additional five SSP2-4.5 CESM2(WACCM6) simulations. None of the above output is contained in the first five ensemble members of CESM2(WACCM6) SSP2-4.5 simulations.

Name of Variable	Variable Description
CaCO3_form_zint_2	Total CaCO3 formation vertical integral
diatChl_SURF	Diatom chlorophyll surface value
diatC_zint_100m	Diatom carbon 0-100m vertical integral
diazChl_SURF	Diazotroph chlorophyll surface value
diazC_zint_100m	Diazotroph carbon 0-100m vertical integral
DpCO2_2	Atmosphere-ocean difference in the partial pressure of CO2
ECOSYS_IFRAC_2	Ice fraction for ecosystem fluxes
ECOSYS_XKW_2	Gas transfer velocity computed based on wind speed squared for ecosys fluxes
FG_CO2_2	Dissolved inorganic carbon surface gas glux
photoC_diat_zint_2	Diatom carbon fixation vertical integral
photoC_diaz_zint_2	Diazotroph carbon fixation vertical integral
photoC_sp_zint_2	Diatom carbon fixation vertical integral
spCaCO3_zint_100m	Small Phyto CaCO3 0-100m vertical integral
spChl_SURF	Small phyto chlorophyll surface value
spC_zint_100m	Small phyto carbon 0-100m vertical integral
STF_O2_2	Dissolved oxygen surface flux
zooC_zint_100m	Zooplankton carbon 0-100m vertical integral
HMXL_DR_2	Mixed-Layer depth
SSS	Sea surface salinity
SST	Surface potential temperature
SST2	Surface potential temperature**2
XMXL_2	Diazotroph carbon fixation vertical integral

Table A9: Daily averaged output from the ocean model in ARISE-SAI-1.5 simulations and all SSP2-4.5 CESM2(WACCM6) simulations.

Name of Variable	Variable Description
aice_d	cce area (aggregate)
aicen_d	ice area, categories
apond_ai_d	melt pond fraction of grid cell
congel_d	congelation ice growth
daidtd_d	area tendency dynamics
daidtt_d	area tendency thermodynamics
dvidtd_d	volume tendency dynamics
dvidtt_d	volume tendency thermodynamics
frazil_d	frazil ice growth
fswabs_d	snow/ice/ocn absorbed solar flux
fswdn_d	down solar flux
fswthru_d	shortwave through the sea ice to ocean
hi_d	grid cell mean ice thickness
hs_d	grid cell mean snow thickness
ice_present_d	fraction of time-avg interval that ice is present
meltb_d	basal ice melt
meltl_d	lateral ice melt
melts_d	top snow melt
meltt_d	top ice melt
sisnthick_d	sea ice snow thickness
sispeed_d	ice speed
sitemptop_d	sea ice surface temperature
sithick_d	sea ice thickness
siu_d	ice x velocity component
siv_d	ice y velocity component
vicen_d	ice volume, categories
vsnon_d	snow depth on ice, categories

466

Table A10: Daily averaged output from the sea-ice model in ARISE-SAI-1.5 simulations and all SSP2-4.5 CESM2(WACCM6) simulations.

Code Availability

CESM2(WACCM6) is freely available from https://www.cesm.ucar.edu/. CESM tag cesm2.1.4-rc.08 was used to carry out the simulations and is also available at: https://zenodo.org/record/7271743#.Y2FBIC-B3qA. Python scripts to generate the case directories with appropriate model tags and output can be found at https://zenodo.org/record/6474201. The code for the SO_2 injections controller can be downloaded from https://zenodo.org/record/6471092#.Yl76rPPMKQc**.**

Data Availability

All the data presented in this manuscript are available at https://zenodo.org/record/6473954#.YmCAwy-B3qA from the CESM2(WACCM6) SSP2-4.5 simulations and at https://zenodo.org/record/6473775#.YmCAdy-B3qA from the ARISE-SAI-1.5 simulations. Complete output from all 10 members of CESM2(WACCM6) SSP2-4.5 simulations and ARISE-SAI-1.5 simulations is freely available the NCAR Climate Data Gateway at https://doi.org/10.26024/0cs0-ev98 and https://doi.org/10.5065/9kcn-9y79 respectively. The ARISE-SAI-1.5 and SSP-4.5 datasets are additionally available for free download through the Amazon/AWS Open Data program. These can be accessed at https://registry.opendata.aws/ncar-cesm2-arise/. We anticipate community analysis of various aspects of the Earth system of the ARISE-SAI-1.5 simulations. There is no obligation to inform the project authors about the analysis you are performing, but it would be helpful to reach out to DV in order to coordinate analysis and avoid duplicate efforts.

Author contribution

JR designed and carried out simulations, compiled output requests, created most of the figures, and drafted the manuscript. DV set-up the injection controller, carried out simulations, created a figure, and wrote parts of the manuscript. DM co-designed the simulations and helped with interpretation of results. DB created the time series of and archived all the data. NR created namelists with desired output and scripts to easily set-up the simulations. BD set up the AWS data hosting site and transferred all the output there. WL analyzed the control simulations and provided targets for the controller. MT and JL gave input to simulation design and data output requests. All authors reviewed the manuscript.

Competing interests

The authors declare that they have no conflict of interest.

Acknowledgements

This material is based upon work supported by the National Center for Atmospheric Research, which is a major facility sponsored by the National Science Foundation under Cooperative Agreement no. 1852977 and by SilverLining through its Safe Climate Research Initiative. The Community Earth System Model (CESM) project is supported primarily by the National Science Foundation. Computing and data storage resources, including the Cheyenne supercomputer (doi:10.5065/D6RX99HX), were provided by the Computational and Information Systems Laboratory (CISL) at NCAR. Cloud storage support is provided through the Amazon Sustainability Data Initiative. We thank two anonymous reviewers for their comments that improved the manuscript (https://doi.org/10.5194/egusphere-2022-125-RC1, https://doi.org/10.5194/egusphere-2022-125-RC2).

References

Andrews, D. G., Holton, J. R., and Leovy, C. B.: Middle atmosphere dynamics. San Diego, CA: Academic Press., 1987.

Beljaars, A. C. M., Brown, A. R., and Wood, N.: A new parameterization of turbulent orographic form drag. Quarterly Journal of the Royal Meteorological Society, 130, 1327–1347. https://doi.org/10.1256/qj.03.73, 2004.

Burgess, M. G., J. Ritchie, J. Shapland and Pielke R. Jr.: IPCC baseline scenarios have over-projected CO2 emissions and economic growth. Env. Res. Lett., 16, 014016, https://doi.org/10.1088/1748-9326/abcdd2, 2021.

Carlson, C. J., and Trisos, C. H.: Climate engineering needs a clean bill of health. Nature Climate Change, 8(10), 843–845, https://doi.org/10.1038/s41558-018-0294-7, 2018.

Chemke, R., Zanna, L., and Polvani, L. M.: Identifying a human signal in the North Atlantic warming hole. Nature Communications, 11(1), 1–7, 2022.

Coburn, J., and Pryor, S. C.: Differential Credibility of Climate Modes in CMIP6, J. Climate, 34(20), 8145-8164, 2021.

Bingaman D. C, Christian V. Rice, Wake Smith and Patrick Vogel: A Stratospheric Aerosol Injection Lofter Aircraft Concept: Brimstone Angel, AIAA 2020-0618, AIAA Scitech 2020 Forum, January 2020.

Danabasoglu, G., Bates, S. C., Briegleb, B. P., Jayne, S. R., Jochum, M., Large, W. G., Peacock S., Yeager S. G.: The CCSM4 ocean component. Journal of Climate, 25, 1361–1389. https://doi.org/10.1175/JCLI-D-11-00091.1, 2012.

Danabasoglu, G., Lamarque, J.-F., Bacmeister, J., Bailey, D. A., DuVivier, A. K., Edwards, J., Emmons L. K., Fasullo J., Garcia R., Gettelman A., Hannay C., Holland M. M., Large W. G., Lauritzen P. H., Lawrence D. M., Lenaerts J. T. M., Lindsay K., Lipscomb, W. H., Mills, M. J., Neale R., Oleson K. W., Otto-Bliesner B., Phillips A. S., Sacks W., Tilmes S., van Kampenhout L., Vertenstein M., Bertini A., Dennis J., Deser C., Fischer C., Fox-Kemper B., Kay J. E., Kinnison D., Kushner P. J, Larson V. E., Long M. C., Mickelson S., Moore J. K., Nienhouse E., Polvani L., Rasch P. J., and W. G. Strand: The Community Earth System Model Version 2 (CESM2). Journal of Advances in Modeling Earth Systems, 12, e2019MS001916. https://doi.org/ 10.1029/2019MS001916, 2020.

Deser, C., Phillips, A., Bourdette, V., Bourdette V., and Teng H.: Uncertainty in climate change projections: the role of internal variability. Clim Dyn 38, 527–546 (2012), https://doi.org/10.1007/s00382-010-0977-x, 2020.

Drijfhout, S., van Oldenborgh, G. J., and Cimatoribus, A.: Is a Decline of AMOC Causing the Warming Hole above the North Atlantic in Observed and Modeled Warming Patterns?, Journal of Climate, 25, 8373–8379, https://doi.org/10.1175/JCLI-D-12-00490.1, http:// journals.ametsoc.org/doi/abs/10.1175/JCLI-D-12-00490.1, 2012.

DuVivier, A. K., Holland, M. M., Kay, J. E., Tilmes, S., Gettelman, A., and Bailey, D. A.: Arctic and Antarctic sea ice mean state in the Community Earth System Model Version 2 and the influence of atmospheric chemistry. Journal of Geophysical Research: Oceans, 125, e2019JC015934. https://doi.org/ 10.1029/2019JC015934, 2020.

Eyring, V., Bony, S., Meehl, G. A., Senior, C. A., Stevens, B., Stouffer, R. J., and Taylor, K. E.: Overview of the Coupled Model Intercomparison Project Phase 6 (CMIP6) experimental design and organization, Geosci. Model Dev., 9, 1937–1958, https://doi.org/10.5194/gmd-9-1937-2016, 2016.

Fasullo, J. T. and Richter, J. H.: Scenario and Model Dependence of Strategic Solar Climate Intervention in CESM, EGUsphere [preprint], https://doi.org/10.5194/egusphere-2022-779, 2022.

Gettelman, A., Mills, M. J., Kinnison, D. E., Garcia, R. R., Smith, A. K., Marsh, D. R., Times, S., Vitt F., Bardeen C. G., McInerny J., Liu H.-L., Solomon S.C., Polvani L. M., Emmons L. K., Lamarque J,-F., Richter, J. H., Glanville A. S., Bacmeister J. T., Philips A. S., Neale R. B., Simpson I. R., DuVivier A. K., Hodzic A., and Randel W. J.: The whole atmosphere community climate model version 6 (WACCM6). Journal of Geophysical Research: Atmospheres, 124, 12,380–12,403. https://doi.org/ 10.1029/2019JD030943, 2019.

Gettelman, A., and Morrison, H.: Advanced two-moment bulk microphysics for global models. Part I: Off-line tests and comparison with other schemes. Journal of Climate, 28, 1268–1287, https://doi.org/10.1175/JCLI-D-14-00102.1, 2015.

Golaz, J.-C., Larson, V. E., and Cotton, W. R.: A PDF-based model for boundary layer clouds. Part I: Method and model description. Journal of the Atmospheric Sciences, 59, 3540–3551, 2002.

Hausfather, Z. and G. P. Peters: Emissions - 'business as usual' story is misleading. Nature 577, 618-620 (2020), doi: https://doi.org/10.1038/d41586-020-00177-3, 2020.

Hunke, E. C., Hebert, D. A., and Lecomte, O.: Level-ice melt ponds in the Los Alamos sea ice model, CICE. Ocean Modelling, 71, 26–42, https://doi.org/10.1016/j.ocemod.2012.11.008, 2013.

Hunke, E. C, Lipscomb, W. H., Turner, A. K., Jeffery, N., and Elliott, S.: CICE: The Los Alamos Sea Ice Model. Documentation and Software User's Manual. Version 5.1. T-3 Fluid Dynamics Group, Los Alamos National Laboratory, Tech. Rep. LA-CC-06-012, 2015.

IPCC: Global Warming of 1.5°C. An IPCC Special Report on the impacts of global warming of 1.5°C above pre-industrial levels and related global greenhouse gas emission pathways, in the context of strengthening the global response to the threat of climate change, sustainable development, and efforts to eradicate poverty [Masson-Delmotte, V., P. Zhai, H.-O. Pörtner, D. Roberts, J. Skea, P.R. Shukla, A. Pirani, W. Moufouma-Okia, C. Péan, R. Pidcock, S. Connors, J.B.R. Matthews, Y. Chen, X. Zhou, M.I. Gomis, E. Lonnoy, T. Maycock, M. Tignor, and T. Waterfield (eds.)]. 2018.

IPCC: Climate Change 2021: The Physical Science Basis. Contribution of Working Group I to the Sixth Assessment Report of the Intergovernmental Panel on Climate Change [Masson-Delmotte, V., P. Zhai, A. Pirani, S. L. Connors, C. Péan, S. Berger, N. Caud, Y. Chen, L. Goldfarb, M. I. Gomis, M. Huang, K. Leitzell, E. Lonnoy, J. B. R. Matthews, T. K. Maycock, T. Waterfield, O. Yelekçi, R. Yu and B. Zhou (eds.)]. Cambridge University Press. 2021.

Kay, J. E., Deser, C., Phillips, A., Mai, A., Hannay, C., Strand, G., Arblaster, J. M., Bates, S. C., Danabasoglu, G., Edwards, J., Holland, M., Kushner, P., Lamarque, J.-F., Lawrence, D., Lindsay, K., Middleton, A., Munoz, E., Neale, R., Oleson, K., Polvani, L., and Vertenstein, M.: The Community Earth System Model (CESM) Large Ensemble Project: A Community Resource for Studying Climate Change in the Presence of Internal Climate Variability, Bulletin of the American Meteorological Society, 96(8), 1333-1349, 2015.

Keil, P., Mauritsen, T., Jungclaus, J. Hedemann C., Olonscheck D., and Ghosh R.:Multiple drivers of the North Atlantic warming hole. Nat. Clim. Chang. 10, 667–671, https://doi.org/10.1038/s41558-020-0819-8, 2020.

Kravitz, B., Caldeira K., Boucher O., Robock A., Rasch P. J., Alterskjær K., Karam D. B., Cole J. N. S.,Curry C. L. , Haywood J. M., Irvine P. J., Ji D., Jones A., Kristjánsson J. E., Lunt D. J., Moore J. C., Niemeier U., Schmidt H., Schulz M., Singh B., Tilmes S., Watanabe S.,Yang S.,and Yoon J-H.: Climate model response from the Geoengineering Model Intercomparison Project (GeoMIP), J. Geophys. Res. Atmos., 118, 8320– 8332, doi:10.1002/jgrd.50646, 2013.

Kravitz, B., MacMartin, D. G., Visioni, D., Boucher, O., Cole, J. N. S., Haywood, J., Jones, A., Lurton, T., Nabat, P., Niemeier, U., Robock, A., Seferian, R., and Tilmes, S.: Comparing different generations of idealized solar geoengineering simulations in the Geoengineering Model Intercomparison Project (GeoMIP), Atmospheric Chemistry and Physics, 21, 4231-4247, https://doi.org/10.5194/acp-21-4231-2021, 2021.

Kravitz, B., MacMartin, D. G., Mills, M. J., Richter, J. H., Tilmes, S., Lamarque, J.-F., J. J. Tribbia, and Vitt, F.: First simulations of designing stratospheric sulfate aerosol geoengineering to meet multiple simultaneous climate objectives. Journal of Geophysical Research: Atmospheres, 122, 12,616–12,634, https://doi.org/10.1002/2017JD026874, 2017.

Larson, V. E., CLUBB-SILHS: A parameterization of subgrid variability in the atmosphere. arXiv:1711.03675v2 [physics.ao-ph], 2017.

Lawrence, D. M., Fisher, R. A., Koven, C. D., Oleson, K. W., Swenson, S. C., Bonan, G., Collier N., Ghimire B., van Kampenhout L., Kennedy D., Kluzek E., Lawrence P. J., Li F., Li H., Lombardozzi D., Riley W. J., Sacks W. J., Shi M., Vertenstein M., Wieder W. R., Xu C., Ali A. A., Badger A. M., Bisht G., van den Broeke M., Brunke M. A., Burns S. P., Buzan J., Clark M., Craig A., Dahlin K., Drewniak B., Fisher J. B., Flanner M., Fox A. M., Gentine P., Hoffman F., Keppel-Aleks G., Knox R., Kumar S., Lenaerts J., Leung L. R., Lipscomb W. H., Lu Y., Pandey A., Pelletier J. D., Perket J., Randerson J. T., Ricciuto D. M., Sanderson B. M., Slater A., Subin Z. M., Tang J., Thomas R. Q., Val Martin M., and Zeng Z: The Community Land Model Version 5: Description of new features, benchmarking, and impact of forcing uncertainty. Journal of Advances in Modeling Earth Systems, 11, 4245–4287. https://doi.org/10.1029/2018MS001583, 2019.

Lee, W. , D. MacMartin, D. Visioni, and Kravitz B.: Expanding the design space of stratospheric aerosol geoengineering to include precipitation-based objectives and explore trade-offs. Earth Syst. Dynam.,11, 1051-1072, https://doi.org/10.5194/esd-11-1051-2020, 2022.

Levis, S., Badger, A., Drewniak, B., Nevison, C., and Ren, X. L.: CLMcrop yields and water requirements: Avoided impacts by choosing RCP 4.5 over 8.5. Climatic Change, 146, 501–515, https://doi.org/10.1007/s10584-016-1654-9, 2018.

Li, H. Y., Wigmosta, M. S., Wu, H., Huang, M. Y., Ke, Y. H., Coleman, A. M., & Leung, L. R.: A physically based runoff routing model for land surface and Earth system models. Journal of Hydrometeorology, 14, 808–828, https://doi.org/10.1175/Jhm-D-12-015.1, 2013.

Li, F., Levis, S., and Ward, D. S.: Quantifying the role of fire in the Earth system—Part 1: Improved global fire modeling in the Community Earth System Model (CESM1). Biogeosciences, 10, 2293–2314. https://doi.org/10.5194/bg-10-2293-2013, 2013.

Li, F., and Lawrence, D. M.: Role of fire in the global land water budget during the twentieth century due to changing ecosystems. Journal of Climate, 30, 1893–1908. https://doi.org/10.1175/JCLI-D-16-0460.1, 2017.

Liu, X., Ma, P. L., Wang, H., Tilmes, S., Singh, B., Easter, R. C., et al.: Description and evaluation of a new four-mode version of the Modal Aerosol Module (MAM4) within Version 5.3 of the Community Atmosphere Model. Geoscientific Model Development, 9, 505–522. https://doi.org/10.5194/gmd-9-505-2016, 2016.

MacMartin, D. G., Kravitz, B., Keith, D. W., and Jarvis, A.: Dynamics of the coupled human-climate system resulting from closed-loop control of solar geoengineering. Climate Dynamics, 43, 243–258. 2014.

MacMartin, D. G., Wang, W., Kravitz, B., Tilmes, S., Richter, J. H., and Mills, M. J.: Timescale for detecting the climate response to stratospheric aerosol geoengineering. Journal of Geophysical Research: Atmospheres, 124, 1233– 1247. https://doi.org/10.1029/2018JD028906, 2019.

MacMartin, D. G., D. Visioni, B. Kravitz, **J. H. Richter**, T. Felgenhauer, W. Lee, D. Morrow, M. Sugiyama, 2022: Scenarios for modeling solar geoengineering, *Proc. Natl. Acad. Sci. U.S.A.*, 119 (33) e2202230119, https://doi.org/10.1073/pnas.2202230119

Maher, N., Milinski, S., and Ludwig, R.: Large ensemble climate model simulations: introduction, overview, and future prospects for utilising multiple types of large ensemble, Earth Syst. Dynam., 12, 401–418, https://doi.org/10.5194/esd-12-401-2021, 2021.

Meehl, G. A., Arblaster, J. M., Bates, S., Richter, J. H., Tebaldi, C., Gettelman, A., et al.: Characteristics of future warmer base states in CESM2. Earth and Space Science, 7, e2020EA001296. https://doi. org/10.1029/2020EA001296, 2020.

Mills, M. J., Schmidt, A., Easter, R., Solomon, S., Kinnison, D. E., Ghan, S. J., … Gettelman, A. (2016). Global volcanic aerosol properties derived from emissions, 1990–2014, using CESM1(WACCM). Journal of Geophysical Research: Atmospheres, 121, 2332– 2348. https://doi.org/10.1002/2015JD024290

Mills, M. J., Richter, J. H., Tilmes, S., Kravitz, B., MacMartin, D. G., Glanville, A. A., Tribbia J. T, Lamarque J-F., Vitt F., Schmidt A., Gettelman A., Hannay C., Bacmeister J. T., and Kinnison, D. E.: Radiative and chemical response to interactive stratospheric sulfate aerosols in fully coupled CESM1(WACCM). Journal of Geophysical Research: Atmospheres, 122, 13,061– 13,078, https://doi.org/10.1002/2017JD027006, 2017.

Moore, J. K., Doney, S. C., Kleypas, J. A., Glover, D. M., and Fung, I. Y.: An intermediate complexity marine ecosystem model for the global domain. Deep Sea Research, 49, 403–462. https://doi.org/10.1016/S0967-0645(01)00108-4, 2002.

Moore, J. K., Doney, S. C., and Lindsay, K.: Upper ocean ecosystem dynamics and iron cycling in a global three-dimensional model. Global Biogeochemical Cycles, 18, GB4028. https://doi.org/10.1029/2004GB002220, 2004.

Moore, J. K., Lindsay, K., Doney, S. C., Long, M. C., & Misumi, K. Marine Ecosystem Dynamics and Biogeochemical Cycling in the Community Earth System Model [CESM1(BGC)]: Comparison of the 1990s with the 2090s under the RCP4.5 and RCP8.5 scenarios. Journal of Climate, 26, 9291–9312. https://doi.org/10.1175/JCLI-D-12-00566.1, 2013.

National Academies of Sciences, Engineering, and Medicine. Reflecting Sunlight: Recommendations for Solar Geoengineering Research and Research Governance. Washington, DC: The National Academies Press. https://doi.org/10.17226/25762, 2021.

O'Neill, B. C., Tebaldi, C., Van Vuuren, D. P., Eyring, V., Friedlingstein, P., Hurtt, G., Knutti R., Kriegler E., Lamarque J-F., Lowe J., Meehl G. A., Moss R., Riahi K., and Sanderson B. M.: The Scenario Model Intercomparison Project (ScenarioMIP) for CMIP6. Geoscientific Model Development, 9(9), 3461–3482, https://doi.org/10.5194/gmd-9-3461-2016, 2016.

Brian C. O'Neill, Elmar Kriegler, Kristie L. Ebi, Eric Kemp-Benedict, Keywan Riahi, Dale S. Rothman, Bas J. van Ruijven, Detlef P. van Vuuren, Joern Birkmann, Kasper Kok, Marc Levy, William Solecki: The roads ahead: Narratives for shared socioeconomic pathways describing world futures in the 21st century, Global Environmental Change, 42, 169-180, https://doi.org/10.1016/j.gloenvcha.2015.01.004, 2017.

Oleson, K. W., and Feddema, J. : Parameterization and surface data improvements and new capabilities for the Community Land Model Urban (CLMU). Journal of Advances in Modeling Earth Systems., 12, https://doi.org/10.1029/2018MS001586, 2019.

Pitari, G., Aquila V., Kravitz B., Robock A., Watanabe S., Cionni I., De Luca N., Di Geonva G., Mancini E., and Tilmes S.: Stratospheric ozone response to sulfate geoengineering: Results from the Geoengineering Model Intercomparison Project (GeoMIP). J. Geophys. Res. Atmos.,119, 2629–2653, https://doi.org/10.1002/2013JD020566, 2014.

Richter, J. H., Sassi, F., and Garcia, R. R.: Toward a Physically Based Gravity Wave Source Parameterization in a General Circulation Model. Journal of the Atmospheric Sciences, 67(1), 136–156, https://doi.org/10.1175/2009JAS3112.1, 2010.

Richter, J. H., Tilmes, S., Mills, M. J., Tribbia, J., Kravitz, B., MacMartin, D. G., Vitt, F., and Lamarque J-F.: Stratospheric dynamical response and ozone feedbacks in the presence of SO2 injections. Journal of Geophysical Research: Atmospheres, 122, 12,557–12,573, https://doi.org/10.1002/2017JD026912, 2017.

687 Scinocca, J., and Mcfarlane N.: The parametrization of drag induced by stratified flow over anisotropic orography.
688 Quarterly Journal of the Royal Meteorological Society, 126, 2353–2394,
689 https://doi.org/10.1256/smsqj.56801, 2000.

690 Simpson, I. R., Tilmes, S., Richter, J. H., Kravitz, B., MacMartin, D. G., Mills, M. J., Fasullo J. T., and Pendergrass
691 A. G.: The regional hydroclimate response to stratospheric sulfate geoengineering and the role of
692 stratospheric heating. Journal of Geophysical Research: Atmospheres, 124, 12587– 12616,
693 https://doi.org/10.1029/2019JD031093, 2019.

694 Simpson, I. R., Bacmeister, J., Neale, R. B., Hannay, C., Gettelman, A., Garcia, R. R., Lauritzen P. H., March D. R.,
695 Mills M. J., Medeiros B., and Richter J. H.: An evaluation of the large-scale atmospheric circulation and its
696 variability in CESM2 and other CMIP models. Journal of Geophysical Research: Atmospheres, 125,
697 e2020JD032835, https://doi.org/ 10.1029/2020JD032835, 2020.

698 Smith, R., Jones P., Briegleb B., Bryan F., Danabasoglu G., Dennis J., Dukowicz J., Eden C., Fox-Kemper B., Gent
699 P., Hecht M., Jayne S., Jochum M., Large W., Lindsay K., Maltrud M., Norton N., Peacock S., Vertenstein
700 M., Year S.: The Parallel Ocean Program (POP) reference manual, Ocean component of the Community
701 Climate System Model (CCSM), LANL Technical Report, LAUR-10-01853, 141 pp., 2010.

702 Tebaldi, C., Debeire, K., Eyring, V., Fischer, E., Fyfe, J., Friedlingstein, P., Knutti, R., Lowe, J., O'Neill, B.,
703 Sanderson, B., van Vuuren, D., Riahi, K., Meinshausen, M., Nicholls, Z., Tokarska, K. B., Hurtt, G., Kriegler,
704 E., Lamarque, J.-F., Meehl, G., Moss, R., Bauer, S. E., Boucher, O., Brovkin, V., Byun, Y.-H., Dix, M.,
705 Gualdi, S., Guo, H., John, J. G., Kharin, S., Kim, Y., Koshiro, T., Ma, L., Olivié, D., Panickal, S., Qiao, F.,
706 Rong, X., Rosenbloom, N., Schupfner, M., Séférian, R., Sellar, A., Semmler, T., Shi, X., Song, Z., Steger,
707 C., Stouffer, R., Swart, N., Tachiiri, K., Tang, Q., Tatebe, H., Voldoire, A., Volodin, E., Wyser, K., Xin, X.,
708 Yang, S., Yu, Y., and Ziehn, T.: Climate model projections from the Scenario Model Intercomparison Project
709 (ScenarioMIP) of CMIP6, Earth Syst. Dynam., 12, 253–293, https://doi.org/10.5194/esd-12-253-2021, 2021.

710 Tilmes, S., Richter, J. H., Kravitz, B., MacMartin, D. G., Mills, M. J., Simpson, I. R., Glanville, A. S., Fasullo, J. T.,
711 Phillips, A. S., Lamarque, J., Tribbia, J., Edwards, J., Mickelson, S., and Ghosh, S.: CESM1(WACCM)
712 Stratospheric Aerosol Geoengineering Large Ensemble Project, Bulletin of the American Meteorological
713 Society, **99**(11), 2361-2371, 2018.

714 Tilmes, S. Mills, M. J., Niemeier, U., Schmidt, H., Robock, A., Kravitz, B., Lamarque, J.-F., Pitari, G., and English,
715 J. M.: A new Geoengineering Model Intercomparison Project (GeoMIP) experiment designed for climate and
716 chemistry models, Geosci. Model Dev., 8, 43–49, https://doi.org/10.5194/gmd-8-43-2015, 2015.

717 Tilmes S., Richter J. H., Mills M. J., Kravitz B., MacMartin D. G., Vitt F., Tribbia J. T., Lamarque J-F.: Sensitivity
718 of aerosol distribution and climate response to stratospheric SO_2 injection locations, Journal of Geophysical
719 Research: Atmospheres, 122, 12,591– 12,615. https://doi.org/10.1002/2017JD026888, 2017.

Tilmes, S., MacMartin, D. G., Lenaerts, J. T. M., van Kampenhout, L., Muntjewerf, L., Xia, L., Harrison, C. S., Krumhardt, K. M., Mills, M. J., Kravitz, B., and Robock, A.: Reaching 1.5 and 2.0 °C global surface temperature targets using stratospheric aerosol geoengineering, Earth Syst. Dynam., 11, 579–601, https://doi.org/10.5194/esd-11-579-2020, 2020.

Tolman, H. L.: User manual and system documentation of WAVEWATCH III TM version 3.14. Technical note, MMAB Contribution, 276, p.220., 2009.

Tye, M. R., Dagon, K., Molina, M. J., Richter, J. H., Visioni, D., Kravitz, B., and Tilmes, S.: Indices of Extremes: Geographic patterns of change in extremes and associated vegetation impacts under climate intervention, Earth Syst. Dynam., 13, 1233-1257, , https://doi.org/10.5194/esd-13-1233-2022, 2022

Visioni, D., MacMartin, D. G., and Kravitz B.: Is Turning Down the Sun a Good Proxy for Stratospheric Sulfate Geoengineering?, Journal of Geophysical Research: Atmospheres, 126, e2020JD033952, 2021a.

Visioni, D., MacMartin, D. G., Kravitz, B., Boucher, O., Jones, A., Lurton, T., Martine, M., Mills, M. J., Nabat, P., Niemeier, U., Séférian, R., and Tilmes, S.: Identifying the sources of uncertainty in climate model simulations of solar radiation modification with the G6sulfur and G6solar Geoengineering Model Intercomparison Project (GeoMIP) simulations, Atmos. Chem. Phys., 21, 10039–10063, https://doi.org/10.5194/acp-21-10039-2021, 2021b.

Visioni, D., Bednarz, E. M., Lee, W. R., Kravitz, B., Jones, A., Haywood, J. M., and MacMartin, D. G.: Climate response to off-equatorial stratospheric sulfur injections in three Earth System Models – Part 1: experimental protocols and surface changes, EGUsphere [preprint], https://doi.org/10.5194/egusphere-2022-401, 2022

Zhang, G. J., and McFarlane, N. A.: Sensitivity of climate simulations to the parameterization of cumulus convection in the Canadian Climate Center general circulation model. Atmosphere-Ocean, 33, 407–446, 1995.

Zhang, Y., MacMartin, D. G., Visioni, D., and Kravitz, B.: How large is the design space for stratospheric aerosol geoengineering?, Earth Syst. Dynam., 13, 201–217, https://doi.org/10.5194/esd-13-201-2022, 2022.